Materials Science Forum Vols. 157-162 (1994) pp 597-610
© (1994) Trans Tech Publications, Switzerland
doi:10.4028/www.scientific.net/MSF.157-162.597
Materials Science Forum Vol. 157-162 (1994) pp. 597-610
© 1994 Trans Tech Publications, Switzerland

ROLLING AND ANNEALING TEXTURES OF BCC METALS

D. Raabe and K. Lücke

Institut für Metallkunde und Metallphysik,
RWTH Aachen, Kopernikusstr. 14, D-52056 Aachen, Germany

Keywords: Low Alloyed, High Alloyed, Steels, Refractory Metals, Texture, Microstructure

ABSTRACT

In the present work the authors very briefly review their current understanding of the evolution of rolling and annealing textures of bcc materials. The results stemming practically only from own experimental work are devided into two main groups. The first group comprises pure bcc transition metals and alloys with a low content of added elements, i.e. mainly low carbon steels but also Ta, Nb, Mo and W. The second group includes high alloyed bcc transition metals, here steels with 10%-17% Cr and with 3% Si. The results on rolling are sucessfully interpreted on the basis of Taylor type theories and those on recrystallization by the current oriented nucleation and growth selection models.

INTRODUCTION

Being studied already since 50 years, the textures of body centered cubic (bcc) transition metals were often considered to be quite similar to each other. Only in the last 15 years, mainly by applying the orientation distribution function (ODF) [1] instead of only pole figures, the studies became thorough enough to reveal characteristic differences between the various bcc metals and alloys and their dependence on the various parameters, e.g. rolling and annealing treatment, starting texture, amount and kind of alloying elements and microstructure (grain shape, shear bands, precipitations).
The emphasis of this brief overview which can consider only very roughly the most important features is laid on ferritic steels since most of the own experimental work as well as that of the literature has been carried out on low carbon, stainless and electrical steels. Only few experiments on high melting bcc refractory metals can be considered, but these do not deviate essentially from those on low-carbon steels. Since in the present short paper only the main features will be discussed, a more thorough treatment will be given in a subsequent paper [2].
The main results supplementing the results given in earlier reviews [3-6] are presented in Table 1. There the rolling and annealing textures of bcc metals and alloys are roughly devided into two groups: group(a) are those of pure bcc transition metals and alloys with a low content of added elements (Fe, low carbon steels, Ta, Nb, Mo, W), and group(b) are those of high alloyed bcc transition metals (here Fe with 10%-17% Cr, Fe with 3% Si).
In the present work all textures were determined by measuring the four incomplete pole figures

All rights reserved. No part of contents of this paper may be reproduced or transmitted in any form or by any means without the written permission of TTP, www.ttp.net. (ID: 193.175.131.12, Max-Planck-Institut für Eisenforschung GmbH, Düsseldorf, Germany-14/11/13,14:03:23)

598 Textures of Materials

Table 1 Main Features of Texture and Microstructure in BCC Metals

		group(a) pure and low alloyed bcc transition metals	**group(b)** alloyed bcc transition metals
measured examples		Fe, low-C steel, Ta, Nb, Mo, W	steels - 10%-17%Cr and 3%Si
hot rolling / initial state	micro-structure	steels : during cooling after hot rolling 100% γ-α transformation (Fe) small globular grains Ta, Nb, Mo, W : initial state as above	no or little γ-α transformation ***center :*** strongly deformed, recovered : flat grains, small recr. fraction ***near-surface :*** large recr. fraction, grain growth: equiaxed, large grains (esp. FeSi)
	texture	through thickness homogeneous nearly random alloyed steel after strip casting as group(a) above	inhomogeneous ***center :*** strong rolling texture, α-and γ-fibre ***near-surface :*** strong shear texture, {110}<001>, ≈{112}<111>
cold rolling	micro-structure	ε<80% : flat grains, blank {001}<110>-{112}<110> and striped {111}<112> grains shear bands increasing with solute carbon content and grain size (FeC, FeSi)	
	texture	increase of α - and γ-fibre orientations through thickness homogeneous **ε<70% :** α-fibre : {001}<110>-{112}<110> γ-fibre : {111}<112> pronounced **ε>70% :** α-fibre : {001}<110>-{112}<110> γ-fibre : {111}<110> pronounced	inhomogeneous *(inherited from hot rolling)* ***center :*** α-fibre : increase, esp. of (inherited) {001}<110> and {112}<110> γ-fibre : formation of {111}<110> ***near-surface :*** α-fibre : rotation of Goss into {001}<110> γ-fibre : rotation of Goss into {111}<112>
annealing	micro-structure	ε<80%: first recrystallized grains in shear bands and close to grain boundaries orientation with work hardening ⇗ weak, e.g. {001}<110> : recovery orientation with work hardening ⇘ strong, e.g. {111}<uvw> : recrystallization	
	texture	decrease of α-fibre {001}<110>-{112}<110>, increase of γ-fibre, esp. {111}<112> Goss increasing with amount of shear bands in deformation microstructure through thickness homogeneous	inhomogeneous *(inherited from rolling)*

Materials Science Forum Vols. 157-162 599

{110}, {200}, {112} and {103} with $Mo_{K\alpha 1}$ radiation in the back reflection mode [7] using a fully automatic high speed goniometer [8] and by deriving from them the ODF f(g) (l_{max}=22) by applying the series expansion method (The orientation g is here given in terms of the Euler angles φ_1,Φ and φ_2) [1]. According to the cubic crystal symmetry and the orthorhombic sample symmetry (RD = rolling direction, ND = normal direction, TD = transverse direction) the textures are presented in the reduced Euler space ($0° \leq \varphi_1, \phi, \varphi_2 \leq 90°$). Since bcc metals tend to develop texture fibres, it is convenient to apply φ_1-sections through the Euler space or to present the orientation density along various fibres. The most important orientations are indicated in figure 1 and the mostly used fibres in table 2.

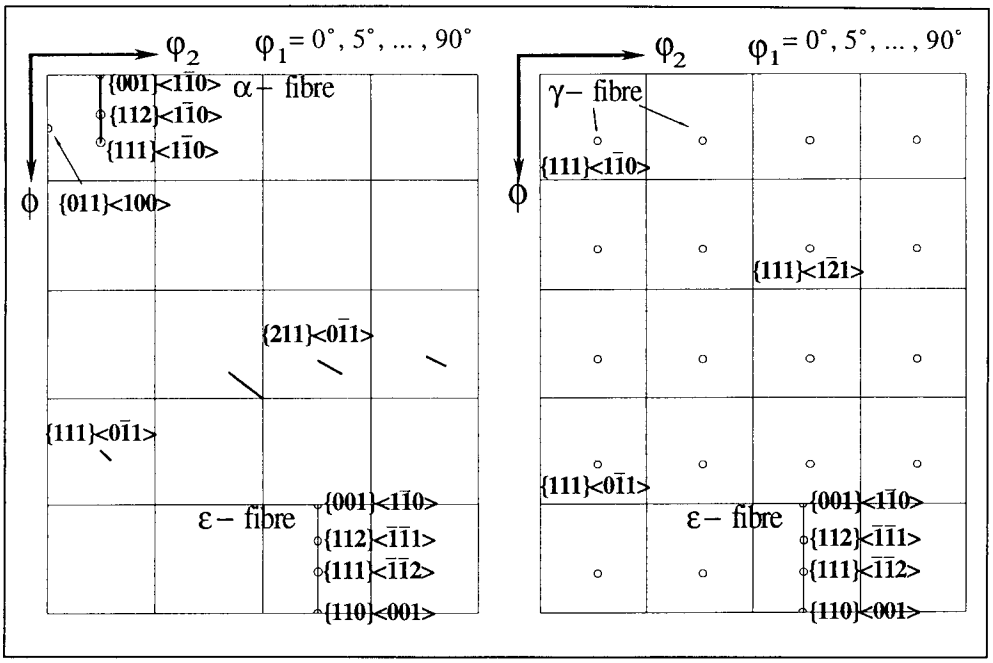

***Figure 1** : Schematical presentation of some orientations and texture fibres which are relevant for bcc materials.*

Table 2 : Relevant fibres for the description of bcc textures.

Fibre	Fibre Axis		Relevant Components belonging to the Fibre
α-fibre	<110>	|| RD	{001}<110> - {112}<110> - {111}<110> (incomplete fibre)
γ-fibre	<111>	|| ND	{111}<110> - {111}<112>
η-fibre	<001>	|| RD	{001}<100> - {011}<100>
ζ-fibre :	<011>	|| ND	{011}<100> - {011}<211> - {011}<111> - {011}<011>
ε-fibre	<110>	|| TD	{001}<110> - {112}<111> - {111}<112> - {011}<100>

Since the textures of bcc metals are often inhomogeneous through the sample thickness, the measurements were carried out in various thickness layers. The inspected layer is described by the parameter s=a/(d/2) with a being the distance of the actual layer from the center layer and d the sample thickness, i.e. s=0 corresponds to the center and s=1 to the surface layer.

600 Textures of Materials

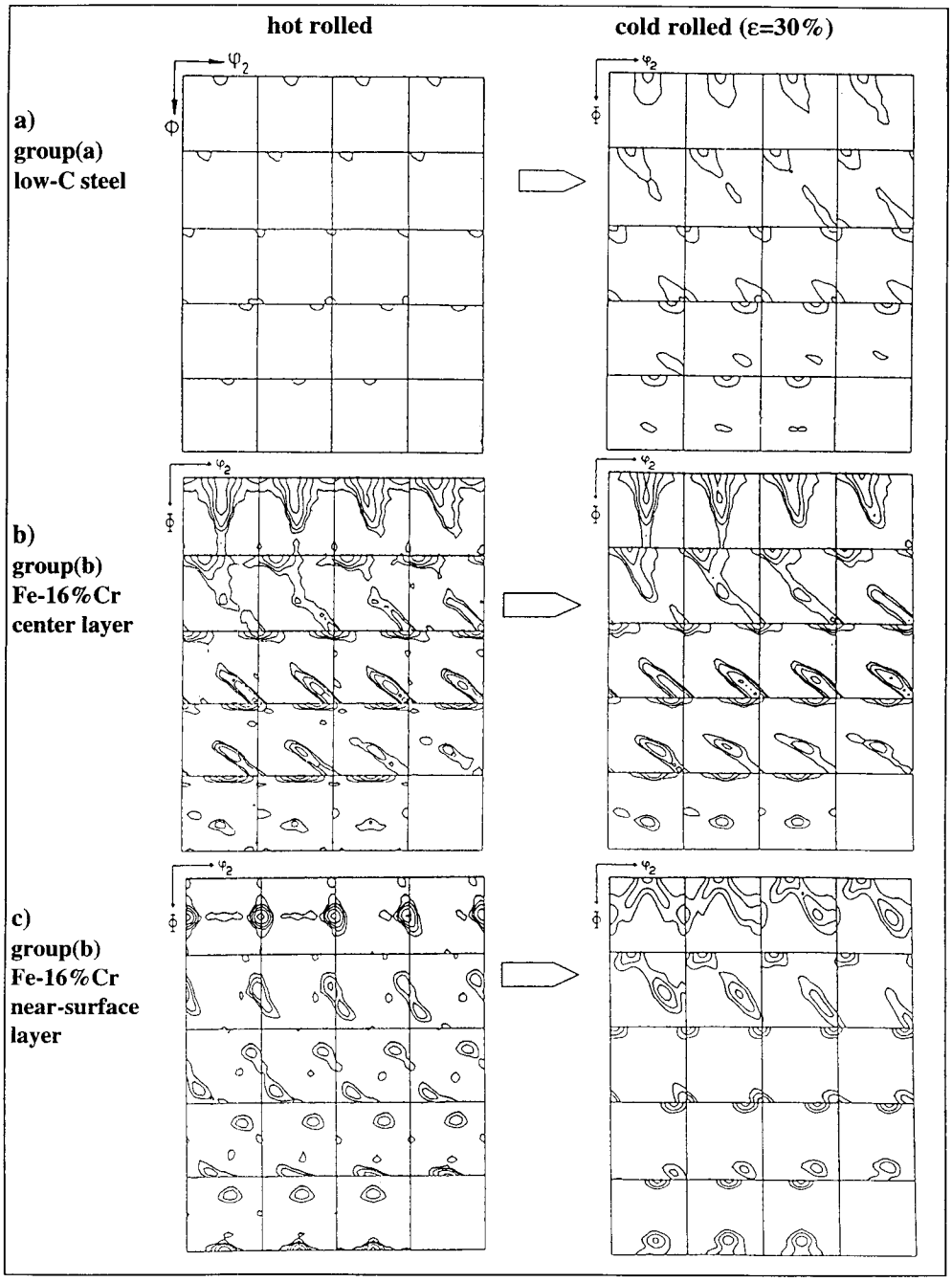

Figure 2: Hot and cold rolling textures. a) group(a), low-C steel, b) group(b), Fe-16%Cr, center layer, c) group(b), Fe-16%Cr, near-surface layer.

Materials Science Forum Vols. 157-162 601

In addition to X-ray measurements, the analysis of electron backscattering patterns (EBSP) obtained by using a scanning electron microscope [9,10] was applied to investigate the formation of textures during deformation and recrystallization also in grain scale.

HOT ROLLING / INITIAL STATE

In their as received initial state the refractory metals reveal an only weak texture without gradient through the sample thickness and will here be classified as group(a). This is also the case for low-C steels (figure 2a) which were obtained as hot bands.

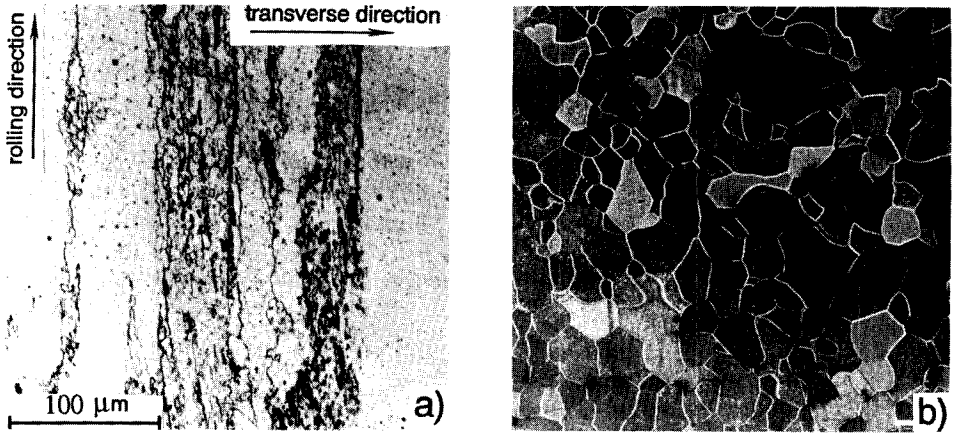

Figure 3 : Micrographs from hot rolled Fe-3% Si, group(b), (a) center, (b) near-surface.

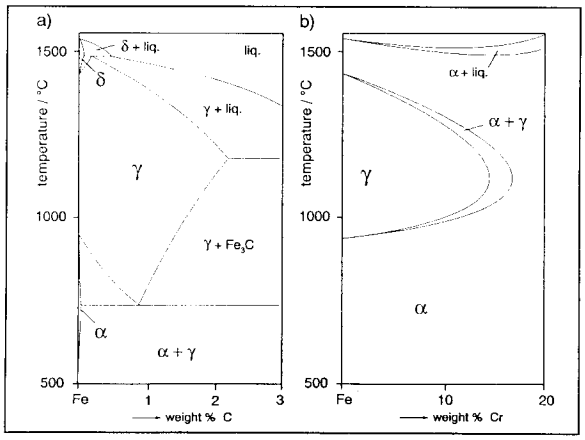

Figure 4: Phase diagrams for group(a), Fe-C (a) and for group(b), Fe-Cr (b).

In contrast to that, the group(b) steels are characterized by a strong gradient in microstructure (figures 3a,b) and texture (figures 2b,c) through the sample thickness. Thoroughly investigated examples are Fe3%Si [13], Fe11%Cr [4] and Fe16% Cr [4,11]. In the center they show a flat and elongated grain morphology with a low recrystallized fraction (figure 3a), whereas at the surface a high amount of recrystallized, equiaxed grains can be seen (figure 3b). Concerning the textures they exhibit in the center layer a strong α-fibre and a weak γ-fibre (figure 2b) and, close to the surface (s≈0.8), a completely different texture, i.e. a strong Goss component {011}<100> and {112}<111> (figure 2c). The difference between the textures as figure 2a on the one side and those of figures 2b and 2c on the other side is the main origin of the sometimes very large differences in the rolling and annealing textures of various steels.

602 Textures of Materials

The reasons for the differences in the hot band structure are differences in the phase diagrams and temperature profiles. The hot rolling for low carbon steels is carried out nearly completely in the γ-phase region (figure 4a) [3,6,11], so that during subsequent cooling nearly 100% γ-α transformation takes place and the texture is thus randomized. Group(b) steels are hot rolled nearly entirely in the α-phase region (figure 4b) so that nearly no phase transformation and thus no randomization by subsequent cooling occurs. This leads for the center layer to the preservation of the above described "cold rolling" type of texture, which results from the there occuring nearly plain strain compression. The surface layers, however, are deformed by strong shear which generates the Goss component and {112}<111> [4,11-14]. Particularly the last hot rolling passes are responsible for the strong inhomogeneity of the strain profile, since here a maximum of the ratio l_d/d which indicates inhomogeneous deformation [15] is achieved (l_d - contact length between roll and sheet, d - thickness of sheet). Due to its lower temperature the stored energy at the sheet surface is increased so that close to the surface recrystallization occurs generating equiaxed grains. In the center layer with its higher temperature and thus lower work hardening only recovery occurs [4,5].
It can thus also be seen, that these gradients become more pronounced with increasing degree of hot rolling and with lowered volume fraction of γ-α transformation [4,5], i.e. in group(b) steels with higher Cr or Si content. If group(a) steels are hot rolled partially in the α-phase region, a texture gradient between surface and center layer is formed, too. On the other hand, if alloyed steels are produced by strip casting they will show the same texture as group(a) steels [16].

COLD ROLLING

The cold rolling textures of all investigated bcc materials (group(a) and (b)) reveal two common features (Table 1): the formation of a strong, incomplete α-fibre between {001}<110> and {111}<110> and the increase of the γ-fibre. This evolution is presented for a low carbon steel (group(a)) in figures 2a and 5a. For $\varepsilon < 70\%$ {001}<110> and {112}<110> are the dominant components on the α-fibre and one sees a weak preference of {111}<112> on the γ-fibre. For $\varepsilon \geq 70\%$ the maximum on the α-fibre is shifted to ≈{112}<110> and that on the γ-fibre from {111}<112> to {111}<110> (figure 5a). In the microstructure the α-grains between {001}<110> and {112}<110> exhibit a blank and the {111}<112> grains a striped appearence so that one can distinguish between both types of grains simply by use of optical microscopy.
Group(b) steels in addition to this basic texture evolution, again reveal a strong texture gradient between center and surface which is inherited from the corresponding hot band texture (figures 2b,c,5b,c). In the center layer (figure 5b) the strong α-fibre already present in the hot band texture with f(g) values being similar to those of the α-fibre of group(a) steels after heavy cold rolling (figure 2b) will be further increased. In the γ-fibre in which the flat and recovered morphology (figure 3a) allows the occurrence of shear in TD between adjacent centre layer grains, mainly a strong {111}<110> orientation develops (figure 5b). Close to the surface, however, the strong initial shear components experience a different texture evolution during cold rolling (figures 2c,5c). The Goss component, which is not stable with respect to plain strain deformation, splits up and rotates towards {001}<110> and {111}<112> (figure 2c) forming there strong maxima (figure 5c).
The development of the rolling textures can be understood in terms of Full Constraints [17] and Relaxed Constraints [18] Taylor type theory (FC- and RC-model) [18-20]. In the FC model each grain is assumed to experience the same strain as macroscopically the whole sample, neglecting the adaptability of the forces at the grain boundaries. Taylor calculations according to the FC-

Materials Science Forum Vols. 157-162 603

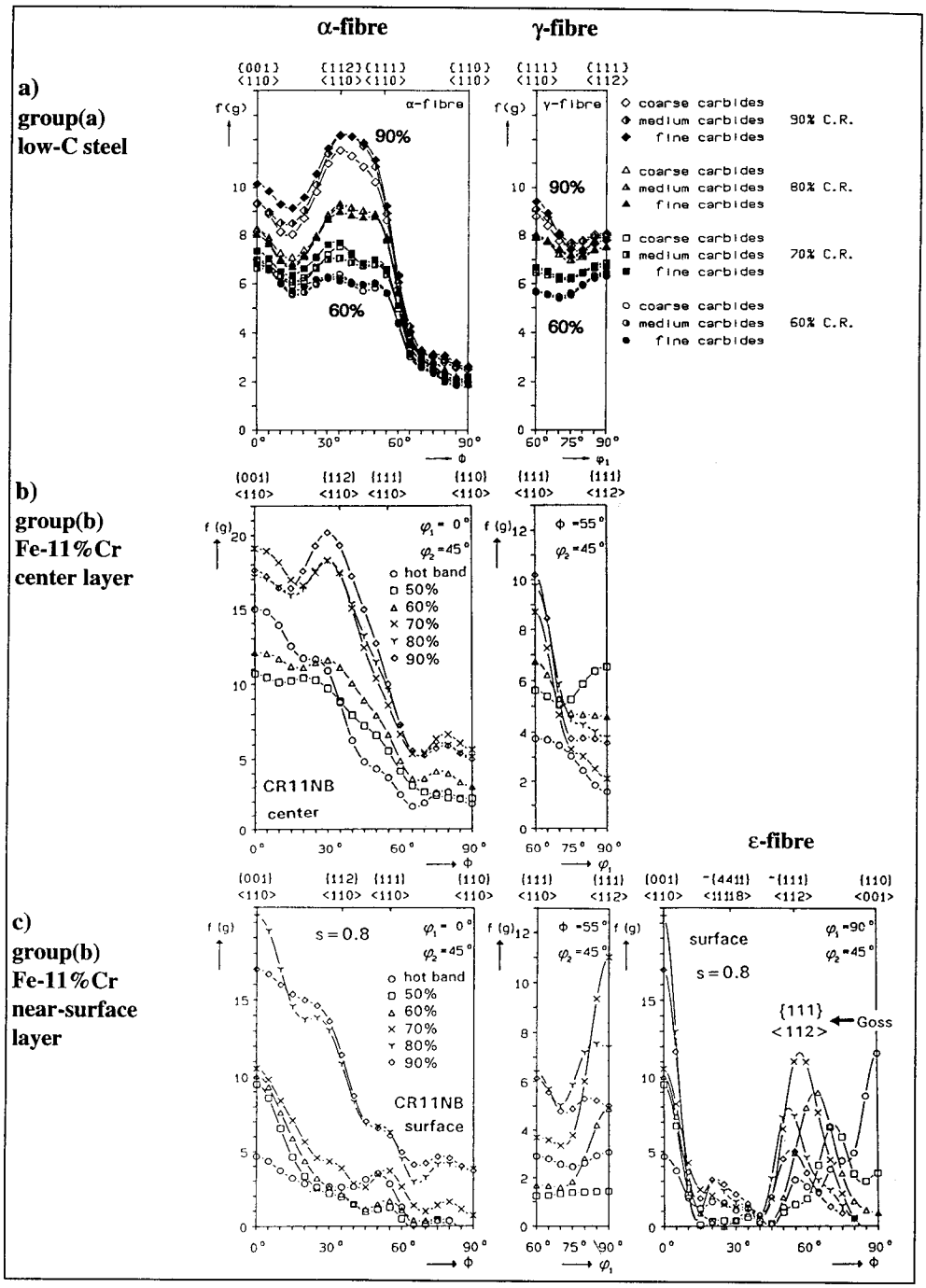

Figure 5 : *Cold rolling texture. a) group(a), low-C steel, b) group(b), Fe-16%Cr steel, center layer, c) group(b), Fe-16%Cr steel, near-surface layer.*

model predict rolling textures with a strong maximum at {11 11 8} <4 4 11>, near {111}<112> which is not corroberated by the above experimental results.
The RC-model assumes that in the grains also shear strains parallel to the rolling plane may occur, at low strains only in RD (lath- or C-model), at high strains additionally in TD (pancake- or SC-model). The first model will cause the formation of the observed {111}<112> orientation the second the rise of {111}<110>. The drop of {111}<112> and the rise of {111}<110> after ε > 70% thus indicates the beginning relaxation of constraints in TD (figure 5a).

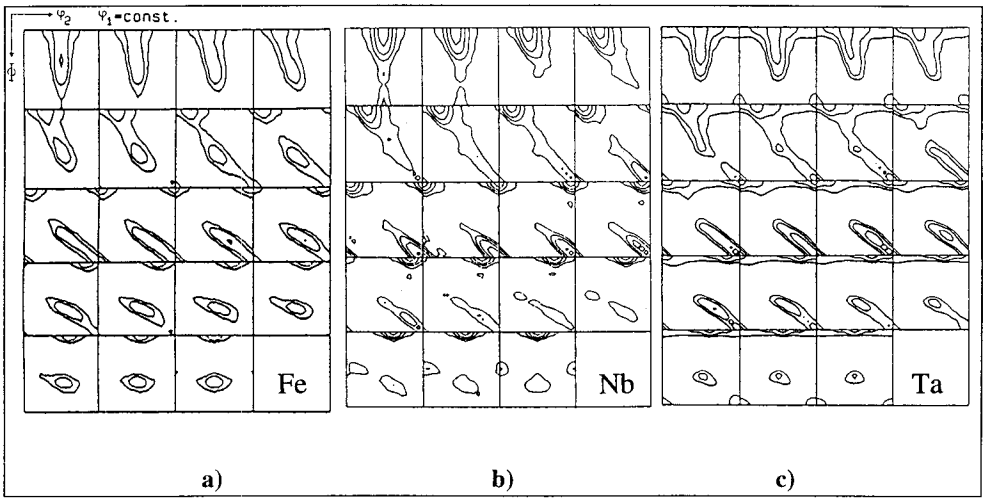

Figure 6 : Cold rolling texture, ε = 70%, group(a), a) Fe, b) Nb, c) Ta.

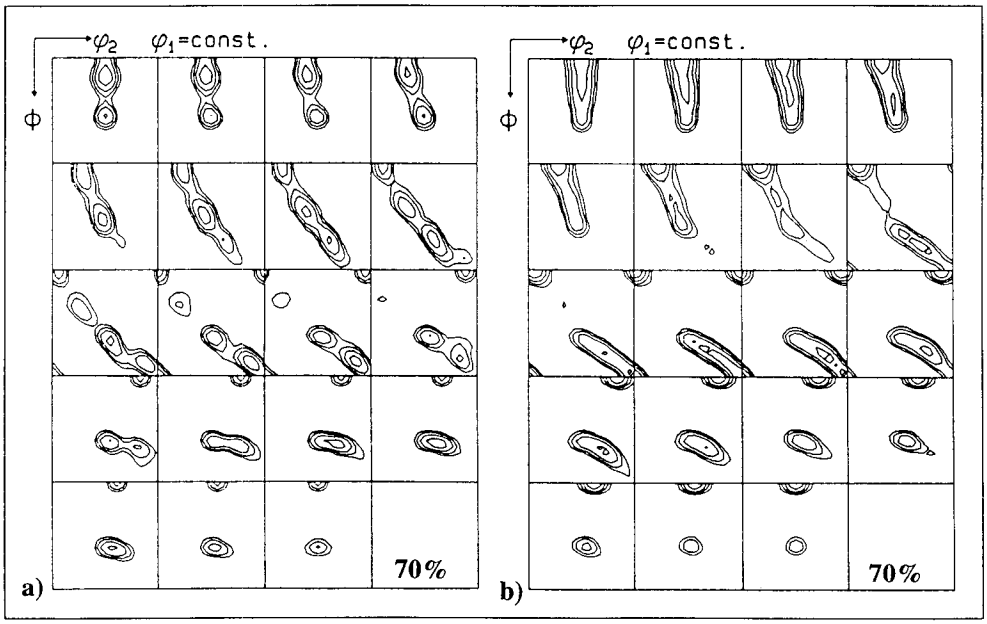

Figure 7 : Taylor model, pancake, a) slip on {110}, b) slip on {110}, {112}, {123}.

In the present work the rolling textures for ε > 70% of the various group(a) materials which were found to be very similar to each other (figures 6a-c) and of group(b) materials (figure 8) were simulated by means of the C- and SC-model (figures 7,9). In the FC model are 5, in the C-model are 4 and in the SC-model are only 3 independent slip systems needed, which are here picked out either from the symmetrically equivalent 12 {110}<111> systems (figure 7a) or from all 48 slip systems yielding <111> slip on all {110}, {112} and {123} planes (figures 7b,9). It can be seen that particulary the latter simulation (figure 9) corresponds very well to the experimentally achieved cold rolling textures (figure 8). If only {110} slip planes are chosen ODFs with strong isolated peaks are obtained (figure 7a). Obviously the fibre type ODFs being typical for bcc metals - in contrast to the peak type ODFs occuring in fcc metals - are due to the activation of additional slip on {112} and {123} planes which means that pencil glide should be a more adequate description of bcc deformation than {110} slip. It is also impressive, how well the texture development on the α-fibre (as presented in figure 8 for group(b) steels) agrees even in details to the predictions of the simulations, if all 48 slip systems are considered (figure 9).

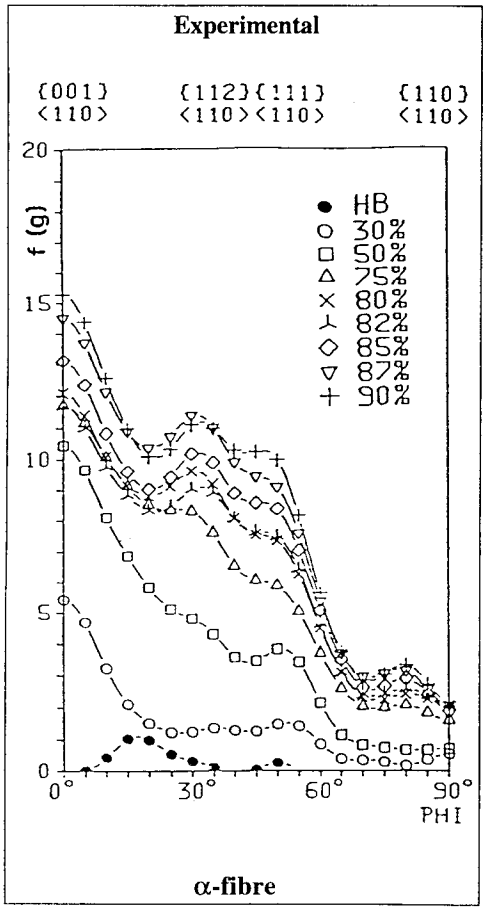

Figure 8 : Cold rolling texture, Fe-16% Cr steel, group(b).

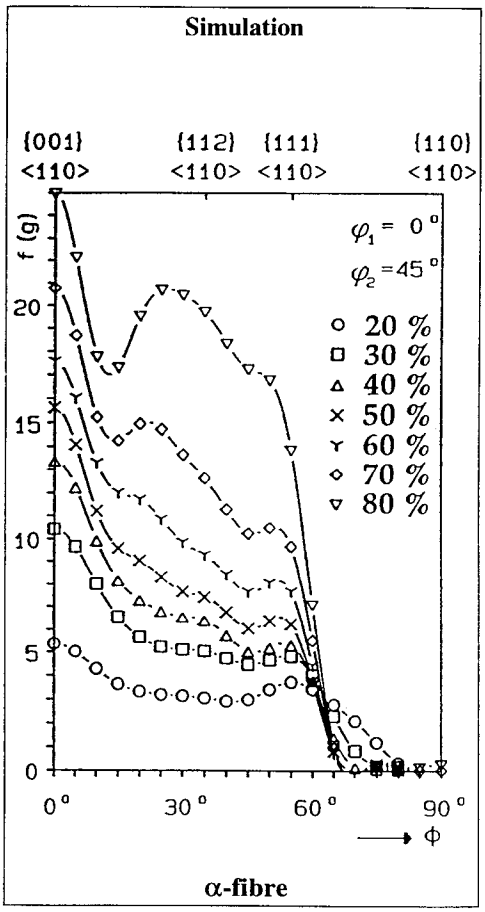

Figure 9 : Taylor simulation, pancake (RC)-model, consideration of slip on {110}, {112} and {123} planes.

ANNEALING

After annealing at homologous temperatures of $T/T_m > 0.4$, all the here investigated bcc metals display after sufficient preceeding cold work ($\varepsilon > 50\%$) a microstructure which in general consists of recrystallized and recovered regions (figure 10). They also reveal common features in the texture development (Table 1).

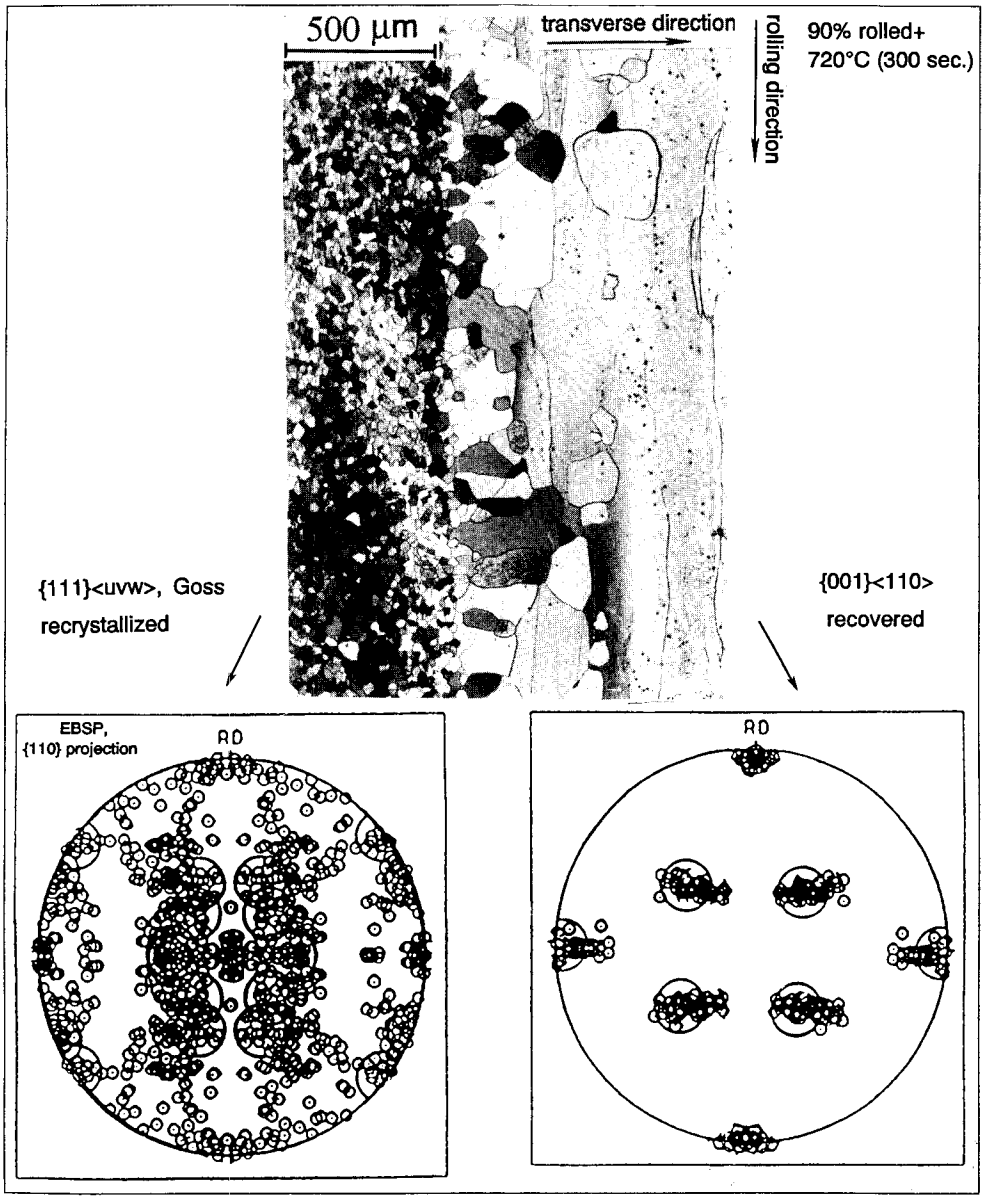

Figure 10 : *Texture and microstructure after cold rolling and annealing, group (a).*

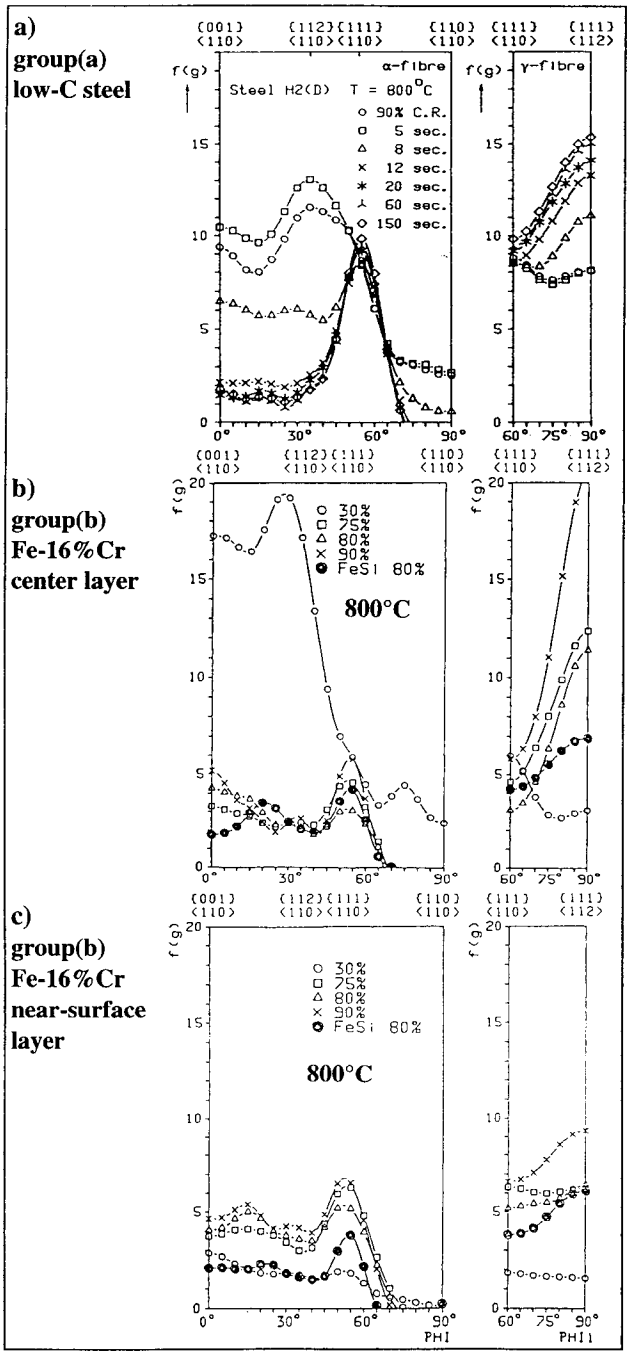

Figure 11 : Annealing textures, a) low-C steel, group(a), b) Fe-16%Cr steel, center layer, c) Fe-16%Cr, near-surface layer.

First the orientation density of the α-fibre between {001}<110> and {112}<110>, especially the strong rolling component {112}<110>, decreases nearly to unity, and second the γ-fibre, particulary {111}<112>, increases. This can be seen for a group(a) steel with low C content in figure 11a. The texture development in group(b) materials basically reveals the same features as in group(a), but the strong texture gradient in group(b) steels stemming already from the hot rolling process leads to inhomogeneous cold rolling textures and thus also influences the annealing textures (figures 11b,c). In the center layer, where the α-fibre exhibits higher orientation densities after cold rolling when compared to the surface, also a stronger γ-fibre is developed. Another feature especially of group(b) annealing textures is the strong occurrence of Goss grains, which is particularly relevant in Fe3%Si (figure 12). Here it can be seen that from a strong {111}<112> rolling texture, in which shear bands are formed during rolling, also a strong Goss orientation results after annealing (figure 12). If a large grain size and a high amount of soluted interstitial elements are present, however, the Goss component is also formed in group(a) materials, e g. in low-C steels.

The formation of recrystallization textures is interpreted mostly on the basis of two models: the model of oriented nucleation and the model of growth selection (or mixed forms). The present main observation, that during recrystallization the orientation density at

608 Textures of Materials

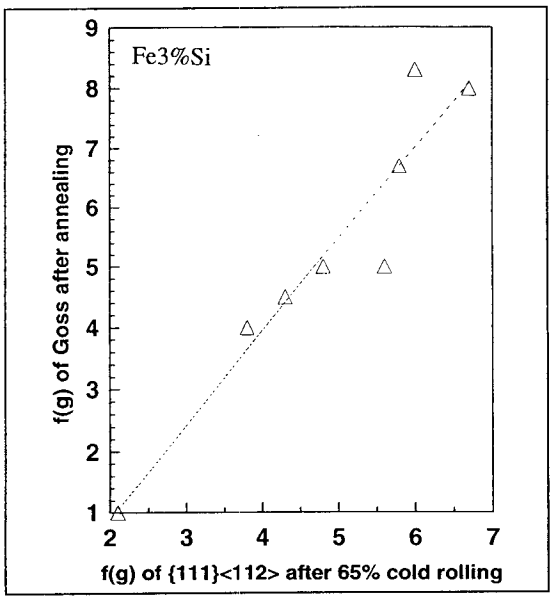

Figure 12 : {111}<112> rolling component leads to a Goss component {110}<001> after annealing.

{111}<112> increases, while simultaneously that of {112}<110> decreases strongly suggests that this texture transition is dominated by growth selection for the following reasons : (i) Since both components are related by a ≈32° rotation about a common <110> axis which, according to Ibe and Lücke [21], is close to a high growth rate relationship, it is assumed that a growth of {111}<112> into {112}<110> is strongly preferred. (ii) For various materials f(g) at {111}<112> increases during recrystallization the more the higher f(g) at {112}<110> in the rolling texture. This shows up especially clearly in figure 13 where the high peak at {111}<112> corresponds to an extremely high preceeding rolling peak at {112}<110>, or in figure 14 where the changes in height of the two peaks during recrystallization are quantitatively related.

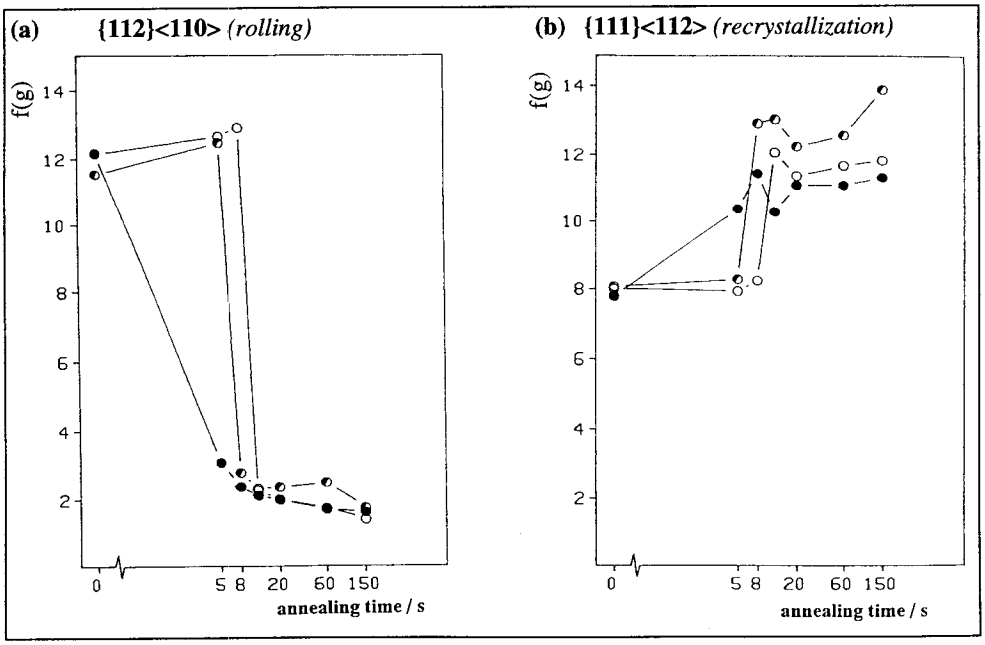

Figure 13 : Growth selection in low carbon steel, three different degrees of dispersion, a) decrease of the {112}<110> rolling component, b) simultaneous increase of the recrystallization component {111}<112>.

Of great importance is also the competition between recrystallization and recovery. The pole figures in figure 10 exhibit the results of single orientation measurements of an annealed Fe-sheet. One sees that the recovered regions have all a {001}<110> orientation whereas the recrystallized ones are γ-grains and to a minor extent Goss. Since the orientation {001}<110> possesses the absolute lowest Taylor factor, it can be concluded that grains with small energy content, i.e. with a low Taylor factor, tend to recover, whereas those with high Taylor factor and thus energy tend to recrystallize (figure 10) [5].

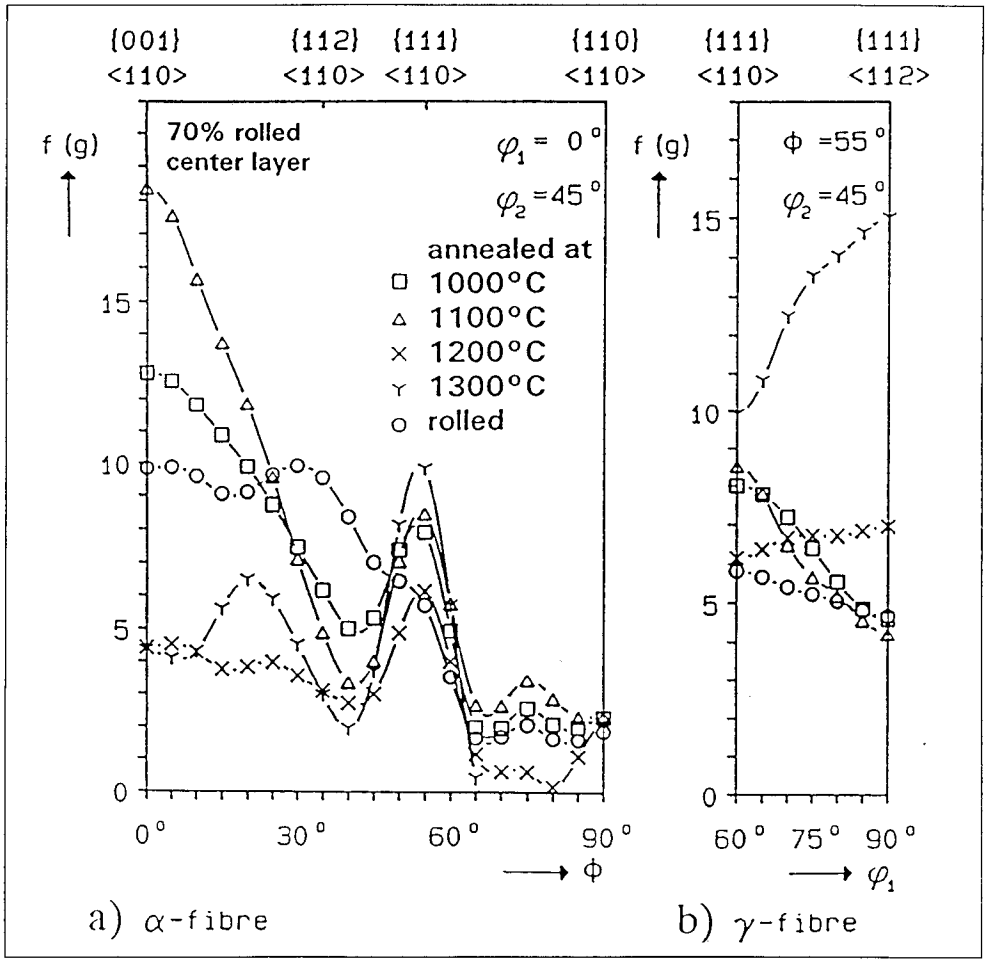

Figure 14 : *Rolled and annealed Tantalum (ε = 70%), a) α -fibre, b) γ -fibre.*

An example for the influence of the annealing temperature on the texture formation of group(a) materials can be seen for 70% rolled Ta (figure 14). While for annealing at 1300°C the above described texture transition from α-fibre to γ-fibre takes place, lower annealing temperatures lead to strong recovery, i.e. to the preservation or even to the enhancement of {001}<110>. This can be explained by the reasonable assumption that the activation energies responsible for grain boundary motion are larger than those for dislocation motion.

Such mobility considerations are also able to explain the effects of particles in the case that

610 Textures of Materials

precipitations are fine enough to exclude particle stimulated nucleation. The superposition of impurity drag [22], caused by dissolution of the carbides during recrystallization, and Zener drag [23] generally leads to the decrease of the strong {111}<112> recrystallization component [24,25].

Finally the appearance of Goss grains will briefly be considered (figure 12). This phenomenon is attributed to nucleation of Goss in shear bands which mainly occur in {111}<112> host grains. Since the shear bands are inclined ≈35° about TD, the shear banding exactly rotates the {111}<112> orientation into the Goss orientation [26]. During annealing the Goss nuclei as parts of the shear bands can grow well into the surrounding deformed {111}<112> grain since their ≈ 35° <110> orientation relationship is again the fast growth relationship. In Fe-Cr alloys where shear banding does not take place because of the small grains size and the interstitial free matrix, the Goss component is much smaller [4]. Here it may be assumed that Goss nucleates in transition zones, which are developed within initial Goss grains adjusting rotations towards {001}<110> with rotations towards {111}<112> (figure 2c) [4]. There are, however, many other effects which influence the Goss with respect to magnitude, orientation scatter and grain size. Because of their great practical importance all these phenomena are thoroughly investigated in a great number of works so that it is not possible to review all aspects in the present short article.

REFERENCES

1. Bunge, H.J.: Texture Analysis in Materials Science, 1982, Butterworths, London
2 Raabe, D., Lücke, K.: to be published
3. Schlippenbach, U.v., Emren, F., Lücke, K.: Acta Met. 1986, 34, No.7, 1289
4. Raabe, D., Lücke, K.: Materials Scien. and Techn. 1993, 9, 302
5. Raabe, D., Lücke, K.: Scripta Met. 1992, 27, 1533
6. Därmann, C.;Mishra, S.; Lücke, K.: Acta Met. 1984, 32, 2185
7. Schulz, L.G. Journal of Applied Physics 1949, 20, 1030
8 Hirsch, J., Loeck, M., Loof, L., Lücke, K.: Proc.ICOTOM 7, 1984, Holland, 765
9. Venables, J., Harland, C.: Phil.Mag. 1973, 27, 1193
10. Engler, O., Gottstein, G.: Steel Research 1992, 63, No.9, 413
11. Hölscher, M.; Raabe, D. Lücke, K.: Steel Research 1991, 62, No.12, 567
12. Raabe, D., Lücke, K., Scripta Met. 1992, 26, No.8, 1221
13. Seidel, L., Hölscher, M., Lücke, K.: Text.and Microstructures 1989, 11 171
14. Hölscher, M., Raabe, D., Lücke, K.: to be published
15. Mao, W.: Ph.D. Thesis. RWTH Aachen, 1988
16. Raabe, D., Hölscher, M., Dubke, M., Pfeifer, H., Hanke, H., Lücke, K.: Steel Research 1993, 64, No.7, 359
17. Taylor, G.I., Journ. Inst. Met. 1938, 62, 307
18. Honneff, H., Mecking, H.: Proc. ICOTOM 6, Tokyo, 1981, ISIJ, 347
19. Raphanel, J.L, van Houtte, P.: Acta Met. 1985, 33, No.8, 1481
20. Hirsch, J., Lücke, K.: Acta Met. 1988, 36, No.11, 2863
21. Ibe, G.; Lücke, K.; Archiv Eisenhüttenwesen 1968, 39, H.9, 693
22. Lücke, K., Detert, K.: Acta Met. 1957, 5, 628
23. Zener, C.: Priv.Communic. to Smith, C.: Trans.AIME 1949, 175, 15
24. Klinkenberg, C., Raabe, D., Lücke, K.: Steel Research 1992, 63, 227
25. Raabe, D., Lücke, K.: Scripta Met. 1992, 26, 19
26. Matsuo, M.: ISIJ Int. 1989, 29, No.10,809

Textures of Materials - ICOTOM 10
10.4028/www.scientific.net/MSF.157-162

Rolling and Annealing Textures of BCC Metals
10.4028/www.scientific.net/MSF.157-162.597